Submitted: 09/09/15
Revised: 04/03/16

Research Article

[1]Department of Physiology, McGill University, Montreal, QC, Canada

Keywords

Sensory adaptation, ambiguity, envelope, power law adaptation, LS: Lateral segment of the electro-sensory lateral line lobe (ELL), CLS: Centro-lateral segment of the ELL, CMS: Centro-medial segment of the ELL

Email Correspondence

zhubo.zhang@mail.mcgill.ca

Zhubo Zhang[1], Maurice J. Chacron

Scale-Invariant Adaptation in Response to Second-Order Electro-Sensory Stimuli in Weakly Electric Fish

Abstract

Background: Natural stimuli can range orders of magnitude, and their encoding by the brain remains a central issue in neuroscience. An efficient way of encoding a natural stimulus is by changing a neuron's coding rule in tandem with changes in the stimulus. This phenomenon is called sensory adaptation. However, sensory adaptation creates ambiguity in the neural code, as different stimuli can produce the same neural response.

Methods: One way to resolve this ambiguity is to encode additional stimulus information through parallel channels. We performed in vivo extracellular recordings from pyramidal cells in two parallel maps, the lateral segment (LS) and the centro-medial segment (CMS), within the hindbrain of the weakly electric fish Apteronotus leptorhynchus, in response to stimuli that resemble the presence of another conspecific.

Results: We found that CMS pyramidal cells generally adapted less strongly than LS cells ($p<0.05$). Signal detection theory confirms that the lesser degree of adaptation leads to a stronger ability to disambiguate between two input stimuli ($p<0.05$). In addition, the time course of adaptation in LS strictly followed a power law while that of CMS followed a power law only for a certain set of stimuli.

Limitations: The design of our study allowed for a stimulus that oscillated only between two distributions. Further studies into the hindbrain's ability to disambiguate the adaptive code will require confusion analysis of a stimulus that changes between more distributions. For confusion studies, cells in different areas can be compared as long as they have receptive fields in similar areas.

Conclusions: Through recording from two parallel segments of the electro-sensory system in the hindbrain, we observed that different segments adapted with different strengths to similar stimuli. Different amounts of adaptation allude to a balance between the need to preserve absolute stimulus information while simultaneously encoding a stimulus efficiently through adaptation.

Introduction

Our senses enable us to experience our surroundings through a multitude of sensations, which are then encoded by the nervous system. One of the most basic ways in which neurons encode information is in their firing rate (1), but a sensory stimulus often contains characteristics that vary over more orders of magnitude than the firing rate can encode. (2) For example, the light intensity outside on a clear winter day is much greater than it is indoors, and our eyes need some time to adjust when moving from one to the other. This adjustment highlights an efficient mechanism for the encoding of light intensity—adaptation. A neuron adapts to a certain stimulus by changing its coding strategy to match the current distribution of the stimulus. (2) In the human visual system, adaptation is more complex than the adaptation of individual neurons, but this process allows individual neurons to encode light intensities over a wide range of magnitudes. Nevertheless, a problem arises with adaptability – ambiguity. Given a certain firing rate, the absolute value of the stimulus it encodes cannot be determined without additional contextual information.

There is much discussion on how the nervous system resolves this problem of ambiguity. In experiments on the fly visual system, Fairhall and colleagues (3) demonstrate that ambiguity can be fully resolved at the level of the individual cell. Other researchers such as Hildebrandt and colleagues (4) describe a circuit-level approach, where the neural circuitry establishes context at the beginning of a stimulus, encoding the remainder of the stimulus relative to it.

Our group has previously suggested a neural computation called parallel coding, where distinct populations of cells encode different features of a stimulus. (5) We believe that parallel coding is another mechanism which can resolve ambiguity—while one population of neurons may adapt to a stimulus, another may not, thus preserving the context of a stimulus. Our model organism is the weakly electric fish Apteronotus leptorhynchus. These fish emit an electric organ discharge (EOD) that can interfere with the EODs of their peers, creating amplitude modulations (AMs). (6) These AMs can indicate the presence of their peers, and are sensed by peripheral electroreceptors located on the surface of the fish. Afferent fibres from the peripheral electroreceptors trifurcate onto three parallel topographical maps in the hindbrain electrosensory lateral line lobe (ELL): the centro-medial (CMS), centro-lateral (CLS), and lateral (LS) segments. (7)

Previous studies have shown that pyramidal cells in these three segments process first-and second-order properties of AMs, such as mean and variance, respectively, relaying them to higher order areas. (5,7) Although adaptation to first-order properties of electrosensory stimuli has been described (5), adaptation to second-order properties has not been characterized. Second-order properties of AMs are defined as the depth of modulation of interference signals, and relate to the distance between the fish and its peer. We will refer to the depth of modulation of an EOD signal as its envelope.

In this paper we compare the responses of LS and CMS cells to step changes in the envelope of the AMs. We chose these areas because of their contrasting frequency tuning properties, acknowledging that the frequency response of CLS cells is intermediate of the two. (7) The frequency tuning of LS and CMS is due in part to the differential expression of small conduc-

tance Ca^{2+} activated K^+ (SK) channels in pyramidal cells (6), where high expression of these channels in LS cells corresponds with its high-pass tuning, and low expression in CMS cells corresponds with its low-pass tuning. Since the spike-triggered SK current is hyperpolarizing, we hypothesized that the amount of adaptation of LS and CMS cells to the AM envelope would also follow the frequency tuning of these areas, where pyramidal cells in LS should adapt more than CMS pyramidal cells. Through peri-stimulus time histogram and signal detection analyses, we found that our results were consistent with this hypothesis. We also characterized the time courses of adaptation between these two areas and found that they could be modelled by a power-law decay for all frequencies in LS, and for frequencies up to 1 Hz in CMS.

Materials & Methods

Surgery & Recording Procedures

All procedures were approved by the McGill University Animal Care Committee. We paralysed the fish with an intramuscular injection of Tubocurarine chloride pentahydrate (Sigma, 1 µg/g body weight), and respirated the fish at a flow rate of 10 mL/min. The fish was kept partially submerged in water, with the top of its head exposed. We then locally anesthetized the site of surgery with 2% lidocaine, removed 6 mm^2 of the skin above the skull, and glued the skull to a metal post to stabilize it. To access the ELL, we first located a major vein known as T0. We then drilled a 2 mm^2 hole through the skull, above the eminentia granularis posterior that lies caudal to T0. (10)

We performed differential extracellular recordings from pyramidal cells in areas LS and CMS with Woods metal electrodes. (11) For area LS, we placed electrodes laterally, halfway from the junction between the cerebellum and eminentia granularis posterior, and rostrally, a third of the way from T0 to the back of the brain, no more than 900 µm from the brain surface. For area CMS, we placed electrodes medially and caudally, halfway from T0 to the back of the brain. These recordings were done at a depth of at least 1200 µm. We identified pyramidal cells based on their responses to a 4 Hz sinusoidal search stimulus—well-isolated cells responded preferentially to a single phase of the stimulus. (7) The signal recorded from the electrodes was amplified (Model 1000 amplifier, A-M systems) and digitized at 16 bits and 10 kHz using a CED Power1401 and Spike2 software. (7)

Stimulus

We stimulated with a sinusoidal electric signal that superimposes with, and creates amplitude modulations (AMs), of the animal's EOD. To phase-lock our output signal with the animal's EOD, we first recorded the EOD with chloridized silver electrodes placed at the head and tail. The zero crossings of the amplified EOD (DAM50, World Precision Instruments) triggered a function generator to create a sine wave at a frequency 40-50 Hz higher than the EOD frequency (Agilent 33220A). The sine waves were multiplied by a waveform, described below as our "stimulus" (MT3 multiplier, Tucker Davis Technologies). The output was then attenuated (LAT45 attenuator, Leader Electronics), and sent to the tank by a stimulus isolator (A395 linear stimulus isolator, World Precision Instruments). These sine waves changed the amplitude of the EOD depending on the polarity of the waveform. The signal was delivered via two electrodes placed 20 cm from the sides of the fish. A dipole was placed approximately 2 mm from the surface of the fish to record the signal sensed by the fish, in order to adjust the attenuation so that the high-low contrast of the AMs was about 10-15%.

Although our stimuli were the EOD-triggered sine waves described above, we will refer to the "stimulus" as the amplitude modulations of the EOD resulting from the sine waves. We used three types of stimuli in our experiments (see below): a 4 Hz AM, randomly modulated 5-15 Hz AMs, and randomly modulated 60-80 Hz AMs. We used the 4 Hz stimulus to test whether our cell in question responded to the stimulus, as described above. The randomly modulated stimuli were designed based on the frequency responses of the segments of the ELL. Areas LS and CLS preferred higher AM frequencies between 40 and 80 Hz, while CMS responded maximally to frequencies below 40 Hz. (8)

All of the stimuli were generated through MATLAB (Mathworks). The 5-15 Hz and 60-80 Hz stimuli were composed of band-pass filtered (fourth-order Butterworth), normally distributed white noise. For these, we modulated the envelope, a second-order property of the AMs, by multiplying the signal with a square wave function that switched between high and low amplitude with frequencies that spanned over three orders of magnitude: 0.05, 0.1, 0.25, 0.5, 1, 2, and 4 Hz for the 5-15 Hz and 60-80 Hz stimuli, and an additional 8 and 16 Hz for the 60-80 Hz stimulus. Each stimulus contained 15-180 cycles of the switch where, between cycles, amplitude modulations came from the same distribution but were uncorrelated. For analysis, we pooled data from both the 5-15 Hz and 60-80 Hz stimuli since the results were identical between the frequency ranges.

Spike Time Extraction

Data analysis was also performed in MATLAB. We first filtered the digital extracellular recording with a high-pass eighth-order Butterworth filter with a cut-off frequency of 0.02 Hz in order to remove low-frequency noise and isolate our spikes for extraction. We selected a time range that corresponded to a single stimulus trial and applied an appropriate threshold above the noise to capture the spike times. We then applied a spike selection algorithm for further isolation from noise. For each time the spike crossed the threshold, we took a window of 0.8 ms centered at the time of crossing and plotted the maximum against the minimum of the signal in the window. From the plot, a neuron's action potentials were seen as a cluster distinctly separate from the noise, and could be selected and isolated. We stored the spike times as a binary sequence with each element corresponding to a bin of width equal to the sampling period of the digitized signal, containing 1 if there was a spike, and 0 if there was none.

Peri-Stimulus Time Histograms

We constructed peri-stimulus time histograms (PSTHs) by averaging each cycle of the switch from low to high variance, for each switch frequency. First, we divided the cycle period into a predetermined number of bins between 40 and 60. For each bin, we summed the number of spikes in time, within a single repeat and also across all repeats, divided by the number of repeats as well as the binwidth. The result was an averaged firing rate over time, centered on the middle of each bin. We spaced the binwidths logarithmically with time, to capture the fast changes in firing rate at the beginning of the switch in variance, and linearly with time for the creation of figures. The results were identical in both binning methods. To prepare the PSTH for fitting, we separated the PSTH into two halves, the first being the neuron's response during low variance, and the second being its response to high variance. Since the stimulus switched between high and low variances periodically, the rapid increase in firing rate followed by a decay due to adaptation when the stimulus switched to high variance was captured entirely within the PSTH corresponding to high variance, and the rapid drop in firing rate followed by an increase when the stimulus switched to low variance was captured within the PSTH corresponding to low variance.

Adaptation Strength

We quantified a cell's adaptation strength by its change in mean firing rate during high envelope for the 0.1 Hz step. We pooled data for both 5-15 Hz and 60-80 Hz carrier frequencies as there was no significant difference between them. To compute the firing rates, we took the difference between the peak firing rate during the first quarter of high envelope, and the firing rate just before the step down to low envelope.

Adaptation Time Course Estimation

We isolated the decay in firing rate during high envelope by discarding the first few bins of the PSTH, if any, that preceded the bin containing the maximum firing rate. If the maximum was attained on more than one bin, we discarded the data up to the last maximum. We then re-centered the PSTH in time so that the first bin corresponded to the bin with the highest firing rate. We fitted the time course of decay in firing rate at high envelope with both exponential (Eq. 3) and power law (Eq. 4) models. Before doing so, we first obtained two estimates of the steady-state firing rate at high

stimulus envelope by fitting the decay with the following models using MATLAB's nlinfit function, using evenly spaced bins in the PSTH:

$$r_{exp}(t)=Ae^{-t/\tau}+C, \quad [1]$$

$$r_{pow}(t)=Bt^{-\alpha}+D, \quad [2]$$

where $r_{exp}(t)$ and $r_{pow}(t)$ are the respective firing rates for the exponential and power law fits, A is a normalizing constant for the exponential model, t is time, τ is the exponential time constant in seconds, B is a normalizing constant for the power law model, α is the power law constant, and C and D are the respective estimated steady-state firing rates for the exponential and power law models.

After obtaining estimates of the steady-state firing rate, we created duplicate PSTHs with logarithmically spaced bins, and subtracted the steady-state estimates obtained from both the above models separately. We then normalized each PSTH with respect to the maximum firing rate, and again fitted the normalized data with the following corresponding models:

$$r_{exp}(t)=Ae^{-t/\tau}, \quad [3]$$

$$r_{pow}(t)=Bt^{-\alpha}, \quad [4]$$

where $r_{exp}(t)$ and $r_{pow}(t)$ are now the normalized respective firing rates for the exponential and power law fits, A is the new normalizing constant for the exponential model, τ is the normalized time constant in seconds, B is the new power law normalizing constant, and α is the normalized power law constant.

Receiver-Operator Characteristic Curves

We quantified the ability of a neuron to distinguish between high and low variance through receiver-operating characteristic (ROC) analysis of a neuron's firing rate. We computed the probability distributions of firing rate for a single cell over the course of a 0.1 Hz switch by separating the time course into 500 ms bins, computing the firing rate during each bin over each repetition, and creating a histogram of those rates. To compute the ability to discriminate an input envelope, we set the distribution of firing rates just before the step up to high envelope as the "false" detection and the distribution at another point in time as the "correct" detection. Using a moving threshold, we computed the probability of correct detection and of false alarm as the area under their respective distributions above the threshold during high envelope, and below the threshold during low envelope. We created ROC curves from these probabilities and quantified discriminability as the area under this curve, where a value of 1 means the cell can discriminate perfectly and 0.5 means that the cell cannot discriminate at all.

To compute the average discriminability of LS cells and CMS cells, we normalized the firing rate probability distributions for each cell with respect to the reference distribution taken from just before the onset of high variance, setting the mean of that distribution to zero and scaling all other values by the standard deviation of the reference. This normalization allowed us to compare firing rate histograms between cells. We computed the ROC curve of each cell separately from these distributions. To compute the average ROC curve, we first rotated all points of the curve clockwise by π/4 radians. We binned the interval [0, √2] into 7 bins, set the "centre" of each bin as the average abscissa value of the points contained in the bin, the mean of the ROC curve as the mean of the ordinate values in that bin, and the 95% confidence intervals of the ROC curve as the 95% confidence intervals of those same ordinate values. These points were then rotated counter-clockwise π/4 radians back to the ROC-style orientation.

Results

We obtained extracellular recordings from 45 pyramidal cells in LS and 32 cells in CMS of the ELL of A. leptorhynchus while we played electrosensory stimuli that mimicked interference signals, or AMs, that are present in the presence of another peer (Fig. 1A, blue and green). We periodically

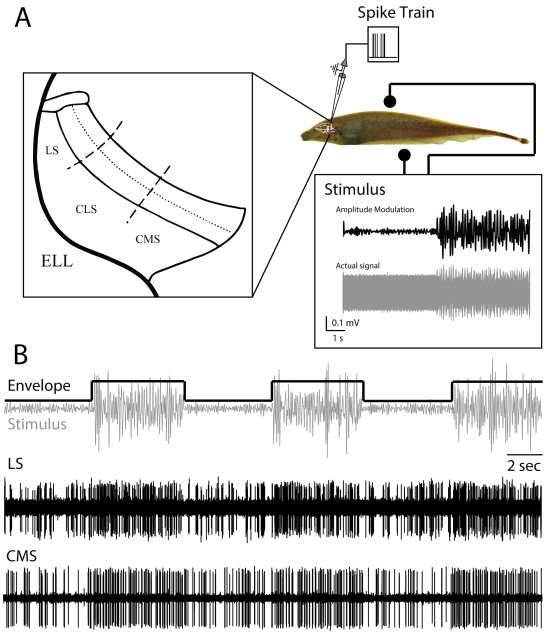

Fig. 1. (A) Schematic of experiment. Electrodes to the side of the fish send sinusoidal stimuli, superimposing with the fish's electric field (bottom right, grey) to create amplitude modulations (bottom right, black). The envelope of the stimulus's amplitude modulations change periodically with time. Extracellular recordings were taken from two areas of the hindbrain known to respond to these modulations, LS and CMS (left). (B) Sample responses of LS and CMS neurons to a stimulus whose envelope (top) steps from low to high with a period of 10 seconds.

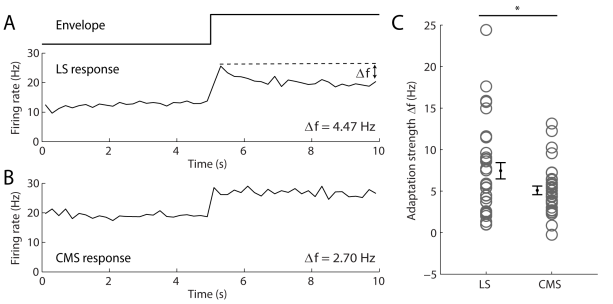

Fig. 2. (A) Averaged PSTH from an LS neuron in response to the stimulus described in Figure 1B. The binwidth used is 500 milliseconds. We define the adaptation strength for each neuron as the difference between the firing rates at the beginning and end of high envelope. (B) Sample response from a CMS neuron (binwidth 500 ms). (C) Changes in firing rates from sample populations in CMS (n=32) are significantly lower than those from LS (n=32, p=0.0377, one-way ANOVA). Black indicates the means and standard error of the means.

switched the depth of modulation, or envelope, of these AMs to simulate different distances between our fish and the mimicked conspecific. Since electromagnetic effects are stronger at closer distances, two fish in close proximity would create AMs with high envelope, and two fish further away lead to AMs with lower envelope. Fig. 1B shows sample responses from LS and CMS cells in response to three repeats for a switching frequency of 0.1 Hz.

Since pyramidal cells in the ELL preferentially respond to specific phases of AMs (8), by averaging over multiple repeats of a high-low modulation cycle we can obtain an averaged PSTH of a cell in response to envelope even when the underlying AMs are uncorrelated. The phase preference of

ELL cells can be grouped into two categories: I-cells that prefer the falling phase of a cycle and E-cells that prefer the rising phase. Since we found no significant difference between the responses of the two types of cells ($p>0.15$ for cells in either segment, in terms of adaptation strength and area under ROC curve), we grouped them together in the presentation of these results. Figs. 2A and 2B show two sample responses from neurons in LS and CMS, respectively. In response to an increase in envelope, both neurons increase their firing rates. However, the LS neuron depicted in Fig. 2A decreases its firing rate over the course of high envelope, suggesting that that neuron adapts. The CMS neuron in Fig. 2B does not noticeably adapt in the same manner. We computed the change in firing rate from the peak to the last bin of the PSTH at high envelope to create a measure of adaptation. Fig. 2C shows aggregate adaptation strengths obtained in this manner. Overall, CMS cells on average maintained their firing rate during high envelope more so than LS cells ($p<0.05$, one-way ANOVA). However, we note that there is a large degree of heterogeneity in adaptation responses, with a smaller number of LS cells and a larger number of CMS cells that do not adapt a considerable amount.

In terms of adaptation, previous experimenters (3, 9-11) have reported that the time course of adaptation resembles a power-law relation rather than an exponential relation with time. We hypothesized that a power-law relation could also describe the time course of ELL pyramidal cell firing rate adaptation in response to changes in envelope. One of the hallmarks of power-law spike frequency adaptation is that the decay is self-similar over different timescales (12), whereas the exponential model of adaptation has a single characteristic timescale and is not

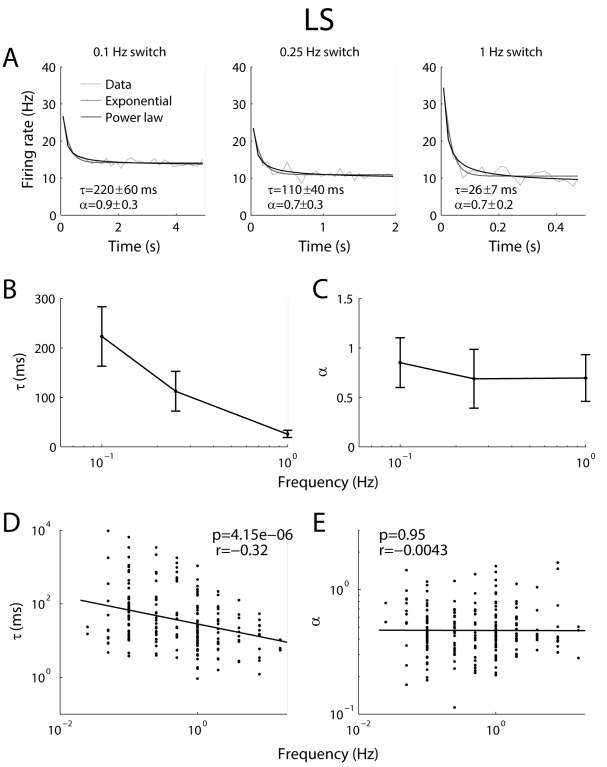

Fig. 3. Exponential and power law fits for LS. (A) Comparison of the decay in firing rate a sample LS cell for three different frequencies of the switch from low to high envelope. We fitted each response with exponential (dark grey) and power-law (black) functions. (B) Exponential time constants for the fits in A, with error bars as 95% confidence intervals. (C) Power-law exponents for the fits in A, with 95% confidence intervals. (D) Time constants of the LS sample population (n=45) as a function of frequency. The axes are logarithmic scale. The solid line is a linear regression fit of the data, the slope of which is significantly different from zero ($p<10\text{-}5$). (E) Power law coefficients of the LS sample population, with a line indicating a linear regression fit. The slope here is not different from zero ($p>0.9$).

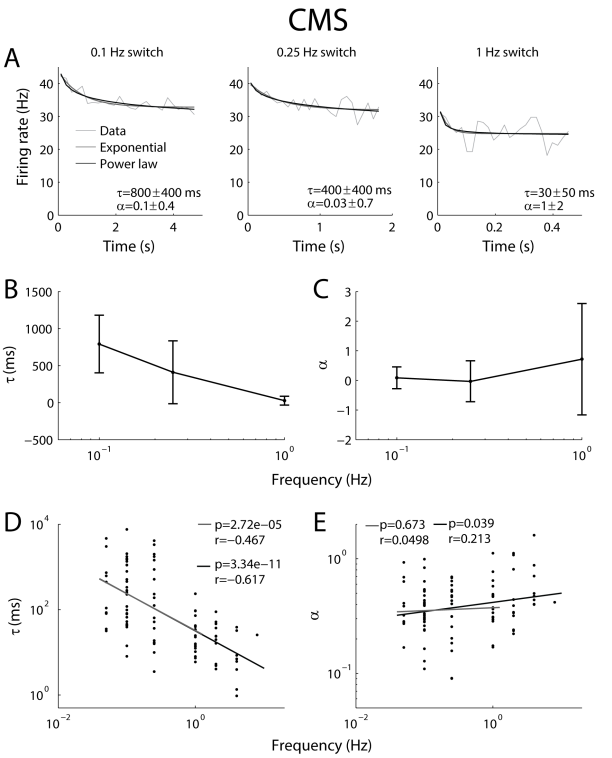

Fig. 4. (A-C) Same format as Figure 3 for CMS. CMS neurons respond weaker than LS neurons to envelope, and adapt less, hence the large error bars that overlap across zero in panels B and C. (D) Time constants for CMS sample population (n=32) with regression fits for frequencies from 0.05 Hz to 1 Hz (grey) and 0.05 Hz to 8 Hz (black). For both frequency ranges, the slopes are significant ($p<10\text{-}4$). (E) Power law constants with linear fits for frequencies up to 1 Hz (grey) and up to 8 Hz (black). The slope for the fit incorporating frequencies from 0.05 Hz to 1 Hz is not significant ($p>0.5$).

self-similar over different timescales. We fitted both exponential and power-law models to the decay in the PSTH in response to changes in envelope over frequencies spanning from 0.05 Hz to 16 Hz. In LS, we found that both models fit very well over a wide range of frequencies (Fig. 3A). However, the time constants of our exponential fits (τ in $e^{-t/\tau}$) were dependent on frequency of switch presented, whereas the power law constants (α in $t^{-\alpha}$) were independent. This held for both single cells (Fig. 3A-C) and the LS sample population (Fig. 3D and 3E), there was a correlation between frequency and time constant of adaptation ($r=-0.317$, $p<10^{-5}$) whereas no correlation was found between frequency and power law constant ($r=-0.004$, $p>0.95$).

Compared with the LS pyramidal cells, the CMS pyramidal cells adapt less to changes in envelope. Therefore, the exponential and power law fits have much more error (Fig. 4A-C). However, the exponential time constant of decay still depends on the frequency of envelope steps both at the individual cell level (Fig. 4B) and across the CMS sample population (Fig. 4D). Estimates for the power law constant of decay is independent of envelope step frequencies up to 1 Hz ($r=0.0498$, $p>0.5$). However, there is a slight positive correlation when considering envelope frequencies above 1 Hz (Fig. 4E, $r=0.213$, $p<0.05$).

Due to the long duration of some of our stimuli, we considered habituation affecting adaptation during and between trials. However, comparisons of the first 30 to the last 30 repeats of the 0.1 Hz stimulus, our longest stimulus at thirty minutes, revealed no significant differences in the time course response. Additionally, the order of stimuli presented were shuffled randomly for each cell that we recorded from a single fish.

To quantify changes in ambiguity as a result of adaptation, we constructed

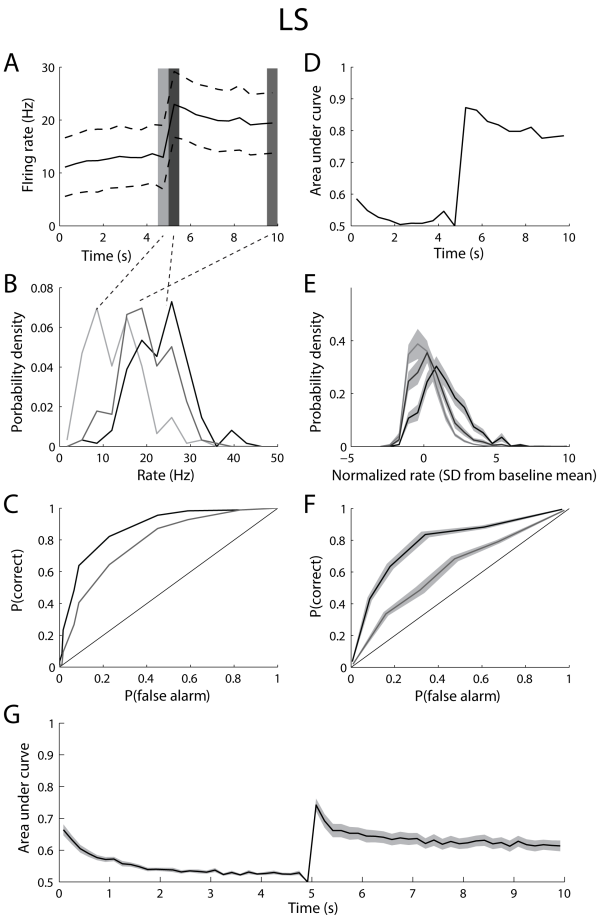

Fig. 5. (A) PSTH for the neuron in Figure 2A displaying the variability of firing rates over each repetition. Dashed lines indicate one standard deviation from the mean. (B) Distribution of firing rates for three sections of the PSTH highlighted in A. (C) ROC curves for the distributions at the beginning (black) and end (grey) of high envelope in comparison to end of low envelope. (D) Areas under the ROC curve across the PSTH in comparison to the end of low envelope. (E) Averaged distributions for the bins highlighted in A across LS sample population (n=32). (F) Averaged ROC curves corresponding to those in C. (G) Averaged area under the ROC curve throughout the entire high-low envelope cycle for LS population. The grey shading in E-G indicate the standard errors of the means.

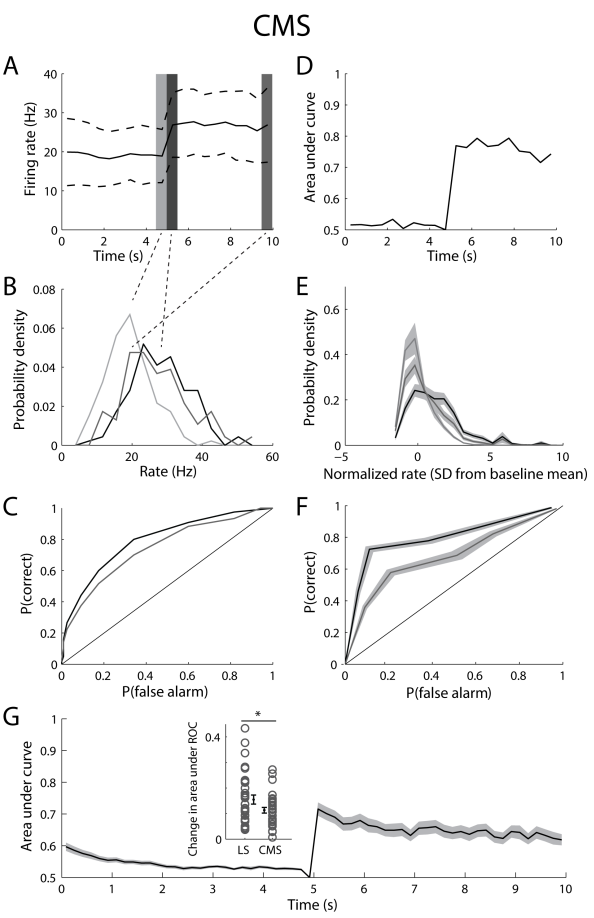

Fig. 6. (A-G) Same format as Figure 5 for CMS population (n=32). (G, inset) Change in area under ROC curve for LS is significantly greater than that of CMS ($p<0.05$, one-way ANOVA).

ROC curves based on the trial-by-trial firing rates of each cell and computed the area under the curves during the course of the 0.1 Hz low-high step in envelope. We took a reference distribution from the distribution of firing rates just before the step up to high envelope, and compared that distribution with the firing rate distributions just after the step up to high envelope and again five seconds later (Figs. 5A,B and 6A,B). We calculated the amount of ambiguity of a cell as the area under the ROC curve at those times (Figs. 5C,D and 6C,D). In both LS and CMS cells, the area under the ROC curve is highest at the onset of high envelope, and decreases as a result of adaptation (Figs. 5E-G, 6E-G). While the steady-state ambiguity at 5 seconds is not significantly different between LS and CMS ($p>0.8$), the drop in the area under the curve across 5 seconds is significantly greater in LS than CMS (Fig. 6G, inset).

Discussion

We investigated the responses of neurons in two segments of the electrosensory hindbrain to changes in second-order properties of naturalistic stimuli and found that generally, these neurons adapted to second-order properties, and the degree of adaptation varied between different areas of the hindbrain. Additionally, our results suggest that the time course of adaptation does not follow a single-timescale exponential decay in the segments sampled. Instead, the two segments adapted differently: one whose time course follows a power law, and another that only resembles a power law for lower frequencies.

The differential expression of SK channels between the segments of the ELL can in part explain the differences in adaptation between the segments. A combination of adapting and non-adapting cells could be a solution to the issue of ambiguity—while non-adapting cells encode the context of a stimulus, adapting cells could code for information relative to that context. Higher expression of SK channels in area LS could also contribute to power law adaptation to changes in envelope. Since increases in Ca^{2+} are associated with increases in synaptic activity, frequent high envelopes during fast high-low cycle lengths increase the build-up of Ca^{2+}, SK channel activation, and, consequently, adaptation. At longer cycle lengths, the long duration of low envelopes decreases pyramidal cell firing, decreasing the build-up of Ca^{2+} and leading to slower adaptive processes during high envelope. This scaling of the adaptation time course with the cycle length of the switch could lead to the scale-invariant characteristic of a power-law decay.

One of the advantages of power law adaptation is that it has the potential to whiten the frequency content of a stimulus. (11) A major theme of neural coding is the decorrelation of input signals between cells, eliminating redundant coding of information and increasing the efficiency of a neural network. (13) Given an input with a non-white frequency content, power law adaptation has the potential to tune an individual neural response to equally represent all input frequencies of the stimulus, maximizing information transfer. (2)

Although the time constants of adaptation in areas CMS and LS vary with the frequency of changes in envelope, the power law constants vary in CMS neurons as well, at least over the range of envelope frequencies

presented. This dependence of the power law constant with frequency in CMS neurons is not present for frequencies up to 1 Hz, suggesting two different mechanisms for envelope processing in the CMS. The low-pass frequency tuning of CMS to envelopes, as suggested by its low amount of adaptation, could render high envelope frequencies (>1 Hz) irrelevant, since these higher envelope frequencies begin to overlap with possible AMs from other fish. We reason that CMS neurons preferentially respond to envelopes of low frequencies indicative of the presence and movement of another fish. In comparison, the frequency tuning of LS to first-order AMs is high-pass (8), allowing more second-order envelope frequencies to be represented in that area.

In our framework of parallel coding, the slowly-adapting CMS cells could serve as a channel to keep track of absolute stimulus features, while the faster-adapting LS cells could allow for encoding of relative stimulus features. One limitation of this model was that there was still a heterogeneity in adaptation in the CMS, where some cells adapted more than others. However, some CMS and even LS cells did not adapt at all, and it could be that these non-adapting cells are the true channels for absolute stimulus information. Further studies investigating adaptation among the different populations of LS and CMS pyramidal cells may reveal the different channels available to disambiguate information provided by spike frequency adaptation.

Acknowledgements

We would like to thank Gary Huang for help with the experiments, and the Natural Sciences and Engineering Research Council of Canada as well as the Fond du Québec: Nature et Technologies, for funding for this project.

References

1. Panzeri S, Brunel N, Logothetis NK, Kayser C. Sensory neural codes using multiplexed temporal scales. Trends Neurosci. 2010;33(3):111-20.
2. Wark B, Lundstrom BN, Fairhall A. Sensory adaptation. Curr Opin Neurobiol. 2007;17(4):423-9.
3. Fairhall AL, Lewen GD, Bialek W, de Ruyter van Steveninck RR. Efficiency and ambiguity in an adaptive neural code. Nature. 2001;412:787-92.
4. Hildebrandt KJ, Ronacher B, Hennig RM, Benda J. A neural mechanism for time-window separation resolves ambiguity of adaptive coding. PLoS Biol. 2015;13(3):e1002096-e.
5. Krahe R, Bastian J, Chacron MJ. Temporal processing across multiple topographic maps in the electrosensory system. J Neurophysiol. 2008;100(2):852-67.
6. Ellis LD, Mehaffey WH, Harvey-Girard E, Turner RW, Maler L, Dunn RJ. SK channels provide a novel mechanism for the control of frequency tuning in electrosensory neurons. J Neurosci. 2007;27(35):9491-502.
7. McGillivray P, Vonderschen K, Fortune ES, Chacron MJ. Parallel coding of first- and second-order stimulus attributes by midbrain electrosensory neurons. J Neurosci. 2012;32(16):5510-24.
8. Chacron MJ, Longtin A, Maler L. Efficient computation via sparse coding in electrosensory neural networks. Curr Opin Neurobiol. 2011;21:752-60.
9. Lundstrom BN, Higgs MH, Spain WJ, Fairhall AL. Fractional differentiation by neocortical pyramidal neurons. Nat Neurosci. 2008;11(11):1335-42.
10. Clarke SE, Naud R, Longtin A, Maler L. Speed-invariant encoding of looming object distance requires power law spike rate adaptation. PNAS. 2013;110(33):13624-9.
11. Pozzorini C, Naud R, Mensi S, Gerstner W. Temporal whitening by power-law adaptation in neocortical neurons. Nat Neurosci. 2013;16(7):942-8.
12. Drew PJ, Abbott LF. Models and properties of power-law adaptation in neural systems. J Neurophysiol. 2006;96(2):826-33.
13. Rieke F. Spikes: exploring the neural code: MIT press; 1999.